

1  
2  
3  
4 **IR Spectroscopy and OH<sup>-</sup> in Silicate Garnet:**

5 **The Long Quest to Document the Hydrogarnet Substitution**

6  
7  
8 Charles A. Geiger<sup>\*,1</sup> and George R. Rossman<sup>2</sup>

9  
10 <sup>1</sup>Department of Chemistry and Physics of Materials  
11 Division Materials Science and Mineralogy  
12 Salzburg University  
13 Jakob Haringer Strasse 2a  
14 A-5020 Salzburg, Austria  
15

16 <sup>2</sup>Division of Geological and Planetary Sciences  
17 California Institute of Technology  
18 Pasadena, CA 91125-2500, USA  
19

20  
21 \*Corresponding author  
22 Tel. (0431) 662-8044-6226  
23 E-mail: [ca.geiger@sbg.ac.at](mailto:ca.geiger@sbg.ac.at)  
24

25  
26 Revised Version #2: American Mineralogist – October 31, 2017  
27  
28  
29  
30  
31  
32  
33  
34  
35

36  
37  
38

## Abstract

39 There has been much research undertaken on structural OH<sup>-</sup> in various nominally anhydrous  
40 minerals including the common silicate garnets (i.e., X<sub>3</sub>Y<sub>2</sub>Si<sub>3</sub>O<sub>12</sub>, where X = Mg, Fe<sup>2+</sup>, Mn<sup>2+</sup> and  
41 Ca and Y = Al, Fe<sup>3+</sup> and Cr<sup>3+</sup>). However, it is still largely not understood where small  
42 concentrations of H atoms are incorporated in the garnet crystal structure. In this work, the IR  
43 single-crystal spectra of end-member or approaching end-member composition andradite, pyrope  
44 and almandine are measured. Both a natural and synthetic andradite sample show a broad,  
45 asymmetric OH-stretching mode at 3563 cm<sup>-1</sup> that splits into two narrower modes at lower  
46 temperatures. They are located at 3575 cm<sup>-1</sup> and 3557 cm<sup>-1</sup> at 80 K with the higher wavenumber  
47 mode being considerably more intense compared to that at lower energy. These results are  
48 analyzed together with published IR spectra of synthetic end-member katoite, pyrope and  
49 almandine also recorded at low temperature. These garnets show similar IR behavior with a broad  
50 OH<sup>-</sup> band at room temperature that splits into two narrower bands at lower temperatures and with  
51 a similar intensity relationship as shown by andradite. This behavior is indicative of the  
52 hydrogarnet substitution. The measured IR spectra of natural almandine- and pyrope-rich (Dora  
53 Maira, Italy) crystals, on the other hand, show different spectroscopic features with several OH<sup>-</sup>  
54 modes that are not consistent with the hydrogarnet mechanism. An analysis of the energy of the  
55 OH<sup>-</sup>-stretching mode is made for various composition hydrogarnet clusters (i.e., X<sub>3</sub>Y<sub>2</sub>(O<sub>4</sub>H<sub>4</sub>)<sub>3</sub>,  
56 where X = Mg, Fe<sup>2+</sup>, Mn<sup>2+</sup> and Ca and Y = Al and Fe<sup>3+</sup>) in terms of crystal-chemical properties  
57 and local atomic configurations. The OH<sup>-</sup> mode energy, which lies roughly between 3660 and  
58 3550 cm<sup>-1</sup> at RT for various end-member garnets, is a function of the mass of the X- and Y-cations  
59 due to mode coupling and/or mixing. In addition, the strength of the chemical bonding between  
60 the X- and Y-cations and the O<sup>2-</sup> anion of the OH<sup>-</sup> dipole plays a role in affecting the wavenumber  
61 of the OH<sup>-</sup>-stretching vibration. OH<sup>-</sup> mode broadening observed in the spectra of end-member  
62 garnets is primarily a result of thermal anharmonic disorder, especially with regard to the light H  
63 cation. OH mode broadening in intermediate solid-solution composition garnets is a function of

64 both thermal effects and variations in local cation configurations around the OH<sup>-</sup> dipole(s).  
65 Published IR spectra of certain high-pressure pyrope-rich garnets, both synthetic and natural, are  
66 analyzed and arguments made that OH<sup>-</sup> can often be incorporated as the hydrogarnet or  
67 hydropyrope substitution. IR spectra similar in appearance, having multiple relatively narrow OH  
68 modes that are distinct from those indicating the hydrogarnet substitution, can be observed for  
69 certain synthetic end-member and various composition natural pyropes from Dora Maira and some  
70 natural spessartines. This indicates that other common OH substitution mechanisms, which have  
71 yet to be determined, can also occur in different silicate garnet.  
72 **Keywords:** hydrogarnet, silicate garnet, OH<sup>-</sup> in minerals, IR spectroscopy, crystal chemistry.

73

## INTRODUCTION

74 There has been much research undertaken on structural OH<sup>-</sup> in nominally anhydrous minerals. A  
75 number of different rock-forming silicates, for instance, have been shown to contain OH<sup>-</sup> in  
76 various, yet minor concentrations. There can be important geological consequences (Keppler and  
77 Smyth, 2006). For example, there has been discussion on how many “oceans of water” could be  
78 present in Earth’s mantle (Bell and Rossman, 1992) with its implications for global geochemical  
79 and geophysical processes. One notable class of silicates that has received much study is the  
80 common silicate garnets (X<sub>3</sub>Al<sub>2</sub>Si<sub>3</sub>O<sub>12</sub> where X = Mg, Fe<sup>2+</sup>, Mn<sup>2+</sup> and Ca and Y = Al, Fe<sup>3+</sup> and  
81 Cr<sup>3+</sup>) and they have been shown to have different OH<sup>-</sup> concentrations arising from various  
82 unknown substitution mechanisms. At low concentration, some researchers speak of OH<sup>-</sup> defects.

83         It terms of studying structural OH<sup>-</sup>, IR single-crystal spectroscopy is generally the  
84 analytical method of choice, because the OH<sup>-</sup> dipole is strongly IR active. The IR spectra of a  
85 large number of natural garnets have been recorded (e.g., Aines and Rossman, 1984; Rossman and  
86 Aines, 1991; Bell and Rossman, 1992; Matsuyk et al., 1998). In spite of this, surprisingly, at least  
87 to the non-expert, is the fact that it is not understood where or how small concentrations of H<sup>+</sup>  
88 atoms are incorporated structurally in the various garnet species. This determination is not easily  
89 made, because the OH<sup>-</sup>-stretching modes cannot be straightforwardly assigned. In addition, some  
90 garnets, such as grossular-katoite compositions especially, show a great variability in the number  
91 of their OH<sup>-</sup> modes (Rossman and Aines, 1991). Of course, diffraction experiments could  
92 theoretically give H positions in a crystal (e.g., Cohen-Addad et al., 1967; Lager et al., 1987), but  
93 at low concentration levels this is not possible. Proton NMR study of synthetic hydrogrossular and  
94 three natural grossulars showed in some cases the presence of four H-atom clusters (hydrogarnet)  
95 and also two H-atom clusters (Cho and Rossman, 1993). Computations have not advanced to the  
96 stage that IR or NMR spectra can be calculated well enough to interpret the experimental results  
97 precisely. In terms of interpreting IR spectra and assigning OH<sup>-</sup> modes, presently one is stuck with  
98 empirical-based comparisons of spectra from different garnets and the possible conclusions that  
99 derive from them.

100           The simple, standard starting point for interpreting IR spectra begins with the classic  
101 hydrogarnet substitution (Aines and Rossman, 1984). That is, one substitutes locally an  $\text{O}_4\text{H}_4^{4-}$   
102 “group” (see Kolesov and Geiger, 2005, for a discussion of  $\text{OH}^-$  mode behavior in katoite) for a  
103  $\text{SiO}_4^{4-}$  one in the silicate garnet crystal structure. The idea derives from early work showing the  
104 existence of “hydrogarnet”. Indeed, end-member katoite,  $\text{Ca}_3\text{Al}_2\text{O}_{12}\text{H}_{12}$ , can be synthesized in the  
105 laboratory and it shows complete solid solution with grossular (Flint et al., 1941). This substitution  
106 mechanism is, because so little is understood, the starting point or “fallback position” that is often  
107 used when attempting to interpret the IR spectra of some silicates and especially silicate garnet  
108 (Aines and Rossman, 1984) with low  $\text{OH}^-$  contents. It remains, however, just an unproven  
109 assumption. It can be concluded, at the present time, that it is not understood precisely how minor  
110  $\text{OH}^-$  is structurally contained in garnet both synthetic and natural.

111           A major obstacle in understanding the nature of  $\text{OH}^-$  in garnet is that natural crystals are  
112 normally solid-solution compositions and, moreover, they have also experienced relatively  
113 complex geologic  $P$ - $T$  histories. Thus, investigations have been made on synthetic crystals that  
114 have simpler chemistries and which can be grown under well controlled  $P(\text{H}_2\text{O})$ - $T$  conditions  
115 (e.g., Geiger et al., 1991; Armbruster and Geiger, 1993; Geiger et al., 1998; Withers et al., 1998;  
116 Mookherjee and Karato, 2010; Geiger et al., in press). Indeed, the results show that synthetic  
117 garnets often, but not always, show simpler IR spectra compared to those of naturals. Another  
118 approach is to measure the spectra of nearly end-member natural garnets with the hope that they  
119 will be simpler than crystals with more complex compositions. These two considerations are one  
120 of the modus operandi for the present work. We present and analyze the IR single-crystal spectra  
121 of natural nearly end-member andradite, pyrope and almandine garnets. The spectra are then  
122 compared with their equivalent synthetic crystals that were grown at high pressure and high  
123 temperature in the laboratory.  $\text{OH}^-$  mode behavior for the hydrogarnet substitution in the various  
124 end-member garnets is interpreted for the first time by considering crystal-chemical properties and  
125 the local atomic configurations around an  $\text{OH}^-$  dipole. This type of analysis is used further in an

126 attempt to assign different OH<sup>-</sup> modes in spectra of various intermediate composition high-  
127 pressure synthetic and natural pyrope-rich garnets.

128

## 129 **SAMPLES AND EXPERIMENTAL METHODS**

### 130 **Garnet samples**

131 The various garnet crystals, both synthetic and natural, measured via IR spectroscopy in this study  
132 are described in Table 1. The precise outcrop locations for three of the pyrope crystals are given in  
133 Simon and Chopin (2001) and their compositions in Geiger and Rossman (1994). The natural near  
134 end-member andradite is from Val Malenco, Italy (collection of GRR) and the synthetic andradite  
135 crystal is described in Armbruster and Geiger (1993) and Geiger et al. (in press). In terms of  
136 almandine, three different natural samples, belonging to the some of the most almandine-rich  
137 crystals found to date, were studied. The geologic occurrence and mineralogical characterization  
138 of two of them are discussed in Woodland et al. (1995) and Aparicio et al. (2012). For IR  
139 investigation, the crystals were slightly ground to two parallel sides to produce thin crystal  
140 platelets and then finely polished.

141

### 142 **FTIR Single-Crystal Spectroscopy**

143 For the IR single-crystal measurements, the preparation and experimental conditions are similar to  
144 those described in Aines and Rossman (1984) and Geiger et al. (1991). A few spectra were obtained  
145 with a Thermo-Nicolet iS50 FTIR with a Continuum microscope accessory with a cryogenic MCT-  
146 A detector and a CaF<sub>2</sub> beam splitter. Most spectra were collected, though, by attaching the doubly  
147 polished crystal platelets over metal pinhole apertures of appropriate size (200 - 600 μm) and  
148 measuring directly in the IR spectrometer sample compartment with an InSb detector. The sample  
149 holder was carefully aligned to yield the strongest signal. Multiple spectra were collected on  
150 different crystal regions that were clear and transparent under the binocular microscope and free  
151 from any observable inclusions.

152 Low-temperature spectra were collected using a Continuum infrared microscope with a 15x  
153 objective and a cryogenic HgCdTe detector. Samples were cooled with liquid nitrogen in a Linkam  
154 FTIR 600 stage.

155

## 156 RESULTS

### 157 **Andradite**

158 The IR spectra of natural end-member andradite (GRR-134) from Val Malenco, Italy, from 296 K  
159 down to 80 K are shown in Figure 1. The broad asymmetric OH<sup>-</sup> band with a peak maximum at  
160 3563 cm<sup>-1</sup> at room temperature (RT) splits into two OH<sup>-</sup> bands that narrow and the more intense  
161 band increases slightly in wavenumber with decreasing temperature. At 80 K, the two peak maxima  
162 are located at 3575 cm<sup>-1</sup> and 3557 cm<sup>-1</sup>. Very weak bands appear at higher wavenumbers in the  
163 spectrum at 80 K. The RT spectrum of synthetic andradite (And #27) is the same as the natural  
164 crystal in terms of the OH<sup>-</sup> band placement (Fig. 1).

165

### 166 **Pyrope**

167 The IR spectra of four different composition pyrope-rich solid-solution crystals from different  
168 geographic locations in the general area of Dora Maira, Italy, are shown in Figure 2. They are  
169 shown with generally decreasing pyrope contents from bottom to top. There is a broadening of the  
170 OH<sup>-</sup> bands as one moves away from close to end-member pyrope into more intermediate  
171 compositions. The spectrum of sample Masueria 2b with the most intense OH<sup>-</sup> modes shows five  
172 well-resolved OH<sup>-</sup> bands located at 3660, 3651, 3641, 3618 (weak) and 3602 cm<sup>-1</sup> and a slight  
173 shoulder on the high wavenumber side of the mode at 3660 cm<sup>-1</sup>. The other pyropes show broadly  
174 similar spectra.

175

### 176 **Almandine**

177 The spectra for the three different almandine samples (Table 1) are shown in Fig. 3. The IR  
178 spectrum of the almandine (FR-3) from Collobrières, France, as described by Woodland et al.

179 (1995), is characterized by an OH<sup>-</sup> band doublet showing possible minor structure. The two main  
180 peaks have maxima at 3641 and 3623 cm<sup>-1</sup>. There is also the possible presence of very weak OH<sup>-</sup>  
181 bands (doublet) centered around ~3590 cm<sup>-1</sup>. The spectrum of almandine from Zlaty Chlum near  
182 Jeseník, Czech Republic, (JF-1) shows weak OH<sup>-</sup> bands at 3562, 3523, 3501, and 3454 cm<sup>-1</sup>.  
183 Another almandine crystal from Collobrières, France, (A-5) shows very weak OH bands similar in  
184 energy to those of the Zlaty Chlum sample.

185

186

## DISCUSSION

### 187 IR Spectra of Compositionally End-Member or Nearly End-Member Garnets

188 **Synthetic and Natural Andradite.** The IR spectrum of end-member andradite (synthetic and  
189 natural) shows a broad asymmetric mode OH<sup>-</sup> at 3563 cm<sup>-1</sup> that splits into two narrower modes at  
190 lower temperatures. We note that other natural andradite crystals can show spectra with more than  
191 one OH<sup>-</sup> band (Amthauer and Rossman, 1998; Adamo et al., 2009; Geiger et al., in press), but  
192 many show this intense band at 3563 cm<sup>-1</sup>.

193

194 **Natural Pyrope.** Garnet crystals from the Dora Maira, Italy, area are unique in terms of  
195 composition (Chopin, 1984; Simon and Chopin, 2001), some being very close to end-member  
196 pyrope - Mg<sub>3</sub>Al<sub>2</sub>Si<sub>3</sub>O<sub>12</sub> (e.g., Masueria 2b/MAS2b and Ch-2 - Table 1). There is, though, a range  
197 of compositional variability involving solid solution with almandine and grossular  
198 ([Mg,Fe<sup>2+</sup>,Ca]<sub>3</sub>Al<sub>2</sub>Si<sub>3</sub>O<sub>12</sub>) giving, for example, crystals with about 76 mol % pyrope (i.e., sample  
199 Masueria 2a/MAS 2a - Table 1). Pyrope-rich garnets from Earth's mantle have entirely different  
200 petrologic origins and ranges of composition, containing considerably more grossular and  
201 almandine, as well as sometimes knorringite, components (e.g., Bell and Rossman, 1992; Matsuyk  
202 et al., 1998, as discussed below). The spectra of the four different crystals from Dora Maira are  
203 similar to those presented in Rossman et al. (1989), who listed four OH<sup>-</sup> bands at 3661.5, 3651.0,  
204 3641.3, and 3602.1 cm<sup>-1</sup>. The measurements herein confirm this, but we find, in addition, a weak  
205 OH<sup>-</sup> mode at 3618 cm<sup>-1</sup> as well as a slight shoulder on the high wavenumber side of the mode at

206 3660  $\text{cm}^{-1}$ . There is a clear broadening of the  $\text{OH}^-$  bands with increasing almandine and grossular  
207 content in the garnet (Fig. 2 - spectra bottom to top). The  $\text{OH}^-$  peak intensities are different among  
208 the four samples indicating variable  $\text{OH}^-$  concentrations.

209  
210 **Natural Almandine.** Three different natural almandine samples were examined and they  
211 represent some of the most  $\text{Fe}_3\text{Al}_2\text{Si}_3\text{O}_{12}$ -rich crystals that have been studied to date (cf., sample  
212 JF-1, Table 1, was first studied by IR spectroscopy by Aparacio et al., 2012). The crystals of JF-1  
213 and A-5 show similar IR spectra with OH modes at about 3562, 3523, 3501, and 3454  $\text{cm}^{-1}$  (Fig.  
214 3). The spectrum of almandine FR-3 is different and is characterized by two narrow higher energy  
215 bands at 3641 and 3623  $\text{cm}^{-1}$ . All three garnets show very different  $\text{OH}^-$  modes than the less  
216 almandine-rich Wrangell sample in Aines and Rossman (1984), whose IR spectrum was proposed  
217 to represent “typical” almandine. The intensity of the  $\text{OH}^-$  bands in all these almandines is weak.  
218 The presented spectra show the most  $\text{OH}^-$ -rich parts of various crystals, as some other recorded  
219 spectra show barely visible  $\text{OH}^-$  bands or none at all (i.e., there are variations in the  $\text{OH}^-$  contents).  
220 Low  $\text{OH}^-$  contents appear to be a general characteristic of many natural almandine crystals (also  
221 unpublished results of C.A.G and G.R.R.).

222  
223 **An Analysis of OH-Mode Behavior in the IR Spectra of Garnet**  
224 **The Hydrogarnet Substitution in End-Member Garnets.** Over the years, the IR spectra of a  
225 large number of garnets, both natural and synthetic, have been measured. In many cases, the  
226 observed  $\text{OH}^-$  stretching bands, which may be one or more in number and showing a range of  
227 wavenumbers, have been suggested to represent the hydrogarnet substitution (e.g., Aines and  
228 Rossman, 1984; Geiger et al., 1991; Withers et al., 1998). However, the underlying scientific  
229 arguments for these proposals are effectively non-existent for anything other than hydrogrossular  
230 (katoite), itself. We think, though, that progress in this question can be made using the IR results  
231 from this work, together with spectra of other garnets given in the literature, by analyzing the  
232 nature of the  $\text{OH}^-$  bands in terms of the structural and crystal-chemical properties of garnet.

233 To start the analysis, we consider the IR spectrum of synthetic katoite,  $\text{Ca}_3\text{Al}_2\text{O}_{12}\text{H}_{12}$ , a  
234 non-silicate garnet, which has been studied at temperatures from 293 K (RT) down to 10 K  
235 (Kolesov and Geiger, 2005). Its  $\text{OH}^-$ -mode behavior is well documented and understood at least  
236 between 293 K and 80 K. The spectrum of katoite shows a single intense and broad asymmetric  
237  $\text{OH}^-$ -stretching mode at  $3662\text{ cm}^{-1}$  at RT, which narrows and shifts to higher energies with  
238 decreasing temperature. With further decreasing temperature and first at about 80 K, a second  
239 much less intense OH stretching mode at about  $3600\text{ cm}^{-1}$  appears. This two OH-band pattern  
240 characterizes the IR spectrum of katoite with the notable addition of weaker fine structure  
241 appearing on these two strongest modes below about 80 K. The nature of these fine structure OH  
242 modes is not understood.

243 The IR spectrum of both natural end-member (Val Malenco) and synthetic andradite are  
244 the same in terms of the energy of the single asymmetric  $\text{OH}^-$  mode occurring at  $3563\text{ cm}^{-1}$ . This  
245 agreement is notable and has not been observed before for other natural and synthetic end-member  
246 garnet species to the best of our knowledge. With decreasing temperature, this OH band begins to  
247 narrow and it splits into a more intense higher energy mode and a less intense mode at low  
248 wavenumbers (Fig. 1 & Fig. 4). We think this behavior reflects the hydrogarnet substitution in  
249 andradite for two reasons. First, it is similar to that observed for katoite upon cooling. Second,  
250 both natural end-member and synthetic andradite show the same IR spectrum. Thus, it can largely  
251 be ruled out that OH defects, related to the presence of other garnet chemical components,  
252 especially those containing highly charged elements (e.g.,  $\text{Ti}^{4+}$  - see below), are not found in  
253 significant amounts in both garnets. *P* and *T* conditions of formation between the two samples are  
254 also widely different. The synthetic was grown at  $1200\text{ }^\circ\text{C}$  (Geiger and Armbruster, 1997),  
255 whereas the natural crystal comes from a much lower temperature serpentinite.

256 This interpretation for the IR hydrogarnet signature is further supported by the spectra of  
257 most synthetic hydrothermally-grown pyropes recorded at RT and 80 K (Geiger al., 1991, see,  
258 however, discussion below on other synthetic pyrope crystals). Once again, a relatively broad  
259 asymmetric  $\text{OH}^-$  mode at  $3629\text{ cm}^{-1}$ , at RT splits upon cooling into two narrow bands at 80 K

260 (3638 and 3614  $\text{cm}^{-1}$  - Fig. 4) and they show a similar intensity relationship as the  $\text{OH}^-$ -mode  
261 doublet in katoite and andradite. Synthetic almandine shows a more complex IR spectrum with  
262 two broad OH bands at RT (Fig. 4), but the most intense  $\text{OH}^-$  band at 3613  $\text{cm}^{-1}$ , which we assign  
263 to the hydrogarnet substitution, behaves in a similar manner (Geiger et al., in press) as the three  
264 garnets discussed above. At 80 K, three narrow  $\text{OH}^-$  bands derive from the RT band at 3613  $\text{cm}^{-1}$ .  
265 However, the typical “hydrogarnet” doublet occurs once again and is the most prominent of the  
266 three bands. Finally, the assignment of the respective  $\text{OH}^-$  modes to a hydrogarnet substitution in  
267 the various end-member garnet species is consistent with their wavenumber behavior as based on  
268 their structural and crystal-chemical properties, as discussed next.

269         The cubic silicate garnet structure, space group  $Ia-3d$ , is characterized by three cation sites  
270 (X, Y, and Si) located on special crystallographic sites and a single oxygen anion located at a  
271 general position (i.e., it has positional freedom in  $x$ ,  $y$  and  $z$ ). Katoite has the same space group  
272 and, here, the Si cation is absent and is charged balanced by the presence locally of four  $\text{H}^+$  cations  
273 (i.e., the so-called hydrogarnet substitution). Figure 5 shows the local atomic environment around  
274 a single  $\text{OH}^-$  group that serves as one dipole of the hydrogarnet  $\text{O}_4\text{H}_4$  cluster without a neighboring  
275 Si cation. The oxygen anion is bonded to one Y cation, two X cations and the H atom. The bond  
276 with H gives the stretching vibration of the  $\text{OH}^-$  dipole that is so strongly IR active. It has been  
277 argued or implied in various works that the energy of this OH stretching mode depends on the  
278  $\text{OH}\cdots\text{O}$  length in the garnet, that is, the strength of the hydrogen bonding. The relationship  
279 between  $\text{OH}\cdots\text{O}$  bond length and the vibrational stretching energy of the  $\text{OH}^-$  bond for many  
280 different compounds is well known (e.g., Nakamoto et al., 1955; Libowitzky, 1999). The analyses  
281 show that the  $\text{OH}^-$  stretching energy is not a meaningful function of the  $\text{H}\cdots\text{O}$  length, when it is  
282 greater than about 2.0 Å. In other words,  $\text{OH}^-$  vibrational energies between roughly 3500 and 3700  
283  $\text{cm}^{-1}$  do not give any unique information on the  $\text{H}\cdots\text{O}$  bond length. Indeed, a free  $\text{OH}^-$  dipole is  
284 considered to vibrate at approximately 3560  $\text{cm}^{-1}$  (Libowitzky, 1999). Thus, it makes no sense to  
285 argue that the varying  $\text{OH}^-$ -mode wavenumbers observed for the different end-member garnets are  
286 related to differences in H-bonding lengths (i.e., H bonding is stronger in  $\text{OH}^-$ -bearing andradite

287 than in OH<sup>-</sup>-bearing pyrope, for example). The lack of measurable hydrogen bonding in garnet is  
288 shown, moreover, by the IR spectra made as a function of temperature. For katoite, andradite,  
289 pyrope, and almandine, the most intense OH<sup>-</sup> mode increases in energy with decreasing  
290 temperature, whereas the general observation for H-bonded systems should be just the opposite,  
291 namely H-bonding increases in strength with decreasing temperature.

292 We think, instead, that the OH<sup>-</sup>-bearing vibrational energy in the different end-member  
293 garnets is largely a function of two crystal-chemical properties. The first is atomic mass. Because  
294 the O<sup>2-</sup> anion in hydrogarnet is bonded to three cations and the H atom (Fig. 5), whereby the  
295 former cations are considerably heavier, the energy of the OH<sup>-</sup> stretching vibration will be affected  
296 via mode coupling through the O<sup>2-</sup> anion. That is, the heavier the combined mass of the X- and Y-  
297 cations, the lower the energy of the OH<sup>-</sup> mode. The second important crystal-chemical effect  
298 involves the strength of the X(1)-O, X(2)-O and Y-O bonds. The stronger they are, the weaker the  
299 OH<sup>-</sup> bond will be. This general effect is, for example, well documented in crystal hydrates  
300 containing an alkali or alkaline-earth cation that is bonded to the oxygen anion of an H<sub>2</sub>O  
301 molecule (Lutz, 1988). The observation is, the stronger the cation-oxygen interaction, the weaker  
302 the intramolecular OH bond (i.e., lower energy) of the H<sub>2</sub>O molecule. In terms of chemical  
303 bonding in silicate garnets it has been shown, using calculated bond valences, that Ca-O bonding  
304 in andradite is stronger than Fe<sup>2+</sup>-O bonding in almandine and Mg-O bonding in pyrope  
305 (Armbruster and Geiger, 1993). Thus, the OH bond in andradite will be weakened compared to  
306 that of the latter two garnets.

307 Consider the bond effect in garnet further. Rossman and Aines (1992) argued that end-  
308 member katoite and OH<sup>-</sup>-poor grossular components in a Ca<sub>3</sub>Al<sub>2</sub>(SiO<sub>4</sub>)<sub>1-x</sub>(O<sub>4</sub>H<sub>4</sub>)<sub>x</sub> solid-solution  
309 crystal are characterized by two OH<sup>-</sup> stretching modes at 3660 and 3598 cm<sup>-1</sup> at RT, respectively.  
310 At first glance, this might appear to be at odds with the analysis given above, because the local  
311 atomic configuration for a hydrogrossular and katoite cluster might be considered the same (Fig.  
312 5). However, only the masses of atoms in the clusters are the same but not the Ca-O bond lengths.  
313 In silicate grossular the Ca-O bond lengths are Ca(1)-O(4) = 2.322(1) Å and Ca(2)-O(4) =

314 2.487(1) Å (Geiger and Armbruster, 1997) and in end-member katoite Ca(1)-O(4) = 2.465(2) Å  
315 and Ca(2)-O(4) = 2.511(1) Å (Lager et al., 1987). Ca-O bonding is stronger in grossular than in  
316 katoite (this analysis ignores, of course, the fact that the Ca-O bonds in a local hydrogrossular  
317 cluster should be a bit longer than the Ca-O bonds in the much more prevalent silicate grossular  
318 “matrix”. That is, there is local bond relaxation in the solid solution). Summarizing, OH bonding  
319 will be weaker for hydrogrossular-like clusters than for katoite clusters in a  $\text{Ca}_3\text{Al}_2(\text{SiO}_4)_{1-x}(\text{O}_4\text{H}_4)_x$   
320 solid-solution crystal.

321 The above analysis does not consider thermal effects, which are clearly reflected in the  
322 temperature-dependent IR measurements. Indeed, diffraction measurements made on katoite  
323 (Lager et al., 1987; Lager et al., 2002) at RT show that the H/D atoms are characterized by large  
324 amplitudes of vibration and we think this dynamic behavior causes the OH<sup>-</sup> mode broadening.  
325 Atomic amplitudes of vibration, especially for the light H atom, are damped at lower temperatures,  
326 resulting in substantial OH<sup>-</sup> mode narrowing and then splitting. Kolesov and Geiger (2005)  
327 analyzed the nature of OH<sup>-</sup> mode widths for both IR and Raman spectra in the case of katoite. It  
328 can be argued that the natural (non thermal) half widths for OH modes are less than 20 cm<sup>-1</sup> at  
329 temperatures below 10 K.

330 In conclusion, an analysis of the wavenumber behavior for the single OH<sup>-</sup> stretching mode  
331 at RT, arising from the presence of hydrogarnet ( $\text{O}_4\text{H}_4^{4-}$ ) groups in various garnets, shows that it  
332 should decrease, as observed, in the order katoite (3662 cm<sup>-1</sup>), pyrope (3629 cm<sup>-1</sup>), almandine  
333 (3613 cm<sup>-1</sup>), grossular (3598 cm<sup>-1</sup>), and andradite (3563 cm<sup>-1</sup>).

### 334 335 **OH-Mode Widths and Energies in End-Member and Intermediate Composition Garnets.**

336 The half-widths of the OH<sup>-</sup> stretching band are greater for intermediate composition natural  
337 garnets with two or more different X-cations compared to those of end-member or nearly end-  
338 member compositions having just one predominant X-cation (e.g., Aines and Rossman, 1984).  
339 The modes are broader because of the presence of different local-cation distributions. That is,  
340 static related local-atomic and -structural heterogeneity contributes to mode broadening in addition

341 to atomic thermal effects. This can be illustrated by considering the possible nature of cation  
342 mixing at the X-site, as in a hypothetical  $[\text{Mg}, \text{Fe}^{2+}, \text{Ca}]_3\text{Al}_2\text{Si}_3\text{O}_{12}$  aluminosilicate garnet (Fig. 6).  
343 This figure shows an edge-shared dodecahedral(D)-tetrahedral(T) chain (Fig. 6a) with a  
344 hypothetical distribution of three different X-cations and a local T-D cluster (Fig. 6b) in the garnet  
345 structure, respectively. Every  $\text{SiO}_4$  or  $\text{O}_4\text{H}_4$  group in garnet has two edge-shared and four corner-  
346 shared dodecahedra (a single OH dipole of an  $\text{O}_4\text{H}_4$  group is illustrated in Fig. 5). In the case of an  
347 end-member garnet, the local X-cation environment around every  $\text{O}_4\text{H}_4^{4-}$  group/OH<sup>-</sup> dipole is the  
348 same (i.e. there is no local compositional and structural heterogeneity). However, in the case of  
349 intermediate composition garnets there should be a range of  $\text{O}_4\text{H}_4^{4-}$  groups or OH dipoles  
350 associated with different local X-cation configurations. Each local-atomic configuration will be  
351 characterized by its own “static” structural properties, for example, bond lengths and angles that  
352 vary with the sizes of the cations involved (see general discussion in Bosenick et al., 2000, and  
353 Freeman et al., 2006).

354 In addition, the masses of the X-cations in the various configurations will be different.  
355 These local variations in structural properties and masses will give rise to a distribution of OH<sup>-</sup>  
356 stretching band mode energies (the situation is, for example, not totally dissimilar to that in the  
357 amphiboles, which are much better understood in terms of their OH<sup>-</sup> mode behavior, see e.g.,  
358 Hawthorne and Della Ventura, 2007. Here, separate OH<sup>-</sup> modes can even be used to describe the  
359 distribution of different cations in neighboring M sites). In other words, in terms of Fig. 6a and  
360 with a typical pyrope-rich mantle garnet, for example, there will be statistically a large fraction of  
361 local D(Mg)-T-D(Mg) configurations, but also D(Mg)-T-D( $\text{Fe}^{2+}$ ), D(Mg)-T-D(Ca), D(Ca)-T-  
362 D( $\text{Fe}^{2+}$ ), D(Ca)-T-D(Ca), and D( $\text{Fe}^{2+}$ )-T-D( $\text{Fe}^{2+}$ ) ones. Their relative percentage will depend on  
363 the bulk composition of the crystal and also, importantly, on any energetically preferred  
364 configurations (i.e., possible short-range cation ordering - see Palke et al., 2015). The latter effect  
365 is complex in nature and not understood for garnet. Indeed, there could well be certain preferred  
366 local atomic configurations ( $\text{O}_4\text{H}_4$  or  $\text{SiO}_4$  groups surrounded by a non-random distribution of X-  
367 cations) in intermediate composition garnets. Of the various silicate garnet species, it is only

368 grossular (and possibly andradite) that shows complete solid solution with a hydrogarnet end  
369 member (Flint et al., 1941). Pyrope and almandine, in comparison, show much less tendency  
370 toward a hydrogarnet solid solution. The simple crystal-chemical interpretation for this is that  
371 garnets with the larger Ca cation, and a concomitant larger unit-cell volume (e.g., grossular -  
372 12.529 J/bar vs. pyrope - 11.316 J/bar and almandine - 11.523 J/bar), offer a more “expanded  
373 crystal structure” that allows for considerable incorporation of the larger O<sub>4</sub>H<sub>4</sub> groups.

374 In conclusion, this crystal-chemical-based analysis offers a framework to begin to interpret  
375 OH<sup>-</sup> mode energies and widths related to various hydrogarnet components in both end-member  
376 and intermediate composition garnets. Former works that simply considered a specific OH<sup>-</sup> mode  
377 energy or energies among different garnet species and their compositions in order to identify, say a  
378 common hydrogarnet substitution, are based on wrong premises. Such a simple analysis cannot be  
379 correct. A first attempt to assign OH<sup>-</sup> IR modes for the hydrogarnet substitution in intermediate  
380 garnets, as well as understanding the physical nature of their energies, will now be made.

### 381 382 **The Hydrogarnet and Other OH<sup>-</sup> Substitutional Mechanisms in High-Pressure Garnets.**

383 Considerable effort has focused on investigating OH<sup>-</sup> in synthetic (Geiger et al., 1991; Withers et  
384 al., 1998; Mookerjee and Karato 2010; Thomas et al., 2015) and natural (Bell and Rossman, 1992;  
385 Matsuyk et al., 1998) high-pressure garnets, because the question of the bulk water content in  
386 Earth’s interior is of great geochemical and geophysical interest. We analyze various published IR  
387 spectra in light of the results on end-member garnets and the crystal-chemical analysis given  
388 above.

389 To start, Figure 7 shows the IR spectra for a synthetic end-member pyrope (P-13 - Geiger  
390 et al., 1991) and a high *P-T* (18 GPa and 1800 °C) synthetic solid-solution garnet of composition  
391 (Mg<sub>2.50</sub>Fe<sup>2+</sup><sub>0.59</sub>)(Si<sub>0.06</sub>Al<sub>1.76</sub>Cr<sub>0.08</sub>Fe<sup>3+</sup><sub>0.02</sub>)[SiO<sub>4</sub>] described in Thomas et al. (2015). Both garnets  
392 show the characteristic broad asymmetric OH<sup>-</sup> mode with a maximum at about 3630 cm<sup>-1</sup>. We  
393 conclude that the latter OH<sup>-</sup>-bearing garnet has a hydropyrope-like substitution (i.e., O<sub>4</sub>H<sub>4</sub> groups  
394 surrounded by Mg cations - Fig. 6). This proposal could be tested by measuring this crystal’s IR

395 spectrum at low temperatures to see if the characteristic “OH<sup>-</sup>-doublet” appears. The IR spectra of  
396 other majorite-containing garnets in Thomas et al. (2015) show different spectra which, in some  
397 cases, may reflect variations in composition and, thus, local cation configurations.

398 The IR spectra of natural pyrope garnets are different in appearance. Many various  
399 composition pyrope-rich garnets, deriving from different mantle-rock types, were studied  
400 spectroscopically in detail by Bell and Rossman (1992) and Matsuyk et al. (1998). There is, in  
401 general, good agreement in the observations from both investigations, which are more  
402 mineralogical-petrological in nature and where assignments of the OH<sup>-</sup> modes were not made. OH<sup>-</sup>  
403 -mode behavior is analyzed, here, using structural and crystal-chemical properties as introduced  
404 above.

405 Presently, it is not understood why natural pyropes show spectra with two or three or more  
406 OH<sup>-</sup> modes and with wavenumbers different than that of the single OH<sup>-</sup> mode at 3629 cm<sup>-1</sup>  
407 observed for most synthetic pyropes. Bell and Rossman divide their studied garnets, based on their  
408 characteristic IR spectra and OH<sup>-</sup> mode energies and intensities, into three groups, namely “high-,  
409 middle- and low-wavenumber” types. Matsuyk et al. propose a similar classification with three  
410 main spectral groups labeled as I, II and III, as characterized by their OH<sup>-</sup>-mode wavenumbers of  
411 3645-3662 cm<sup>-1</sup>, 3561-3583 cm<sup>-1</sup> and 3515-3527 cm<sup>-1</sup>, respectively. The IR spectra of three  
412 different pyropes from mantle xenoliths (LAC-40, Lace, S. Africa and RTF-2 and RTF-4  
413 Rietfontein – Bell and Rossman, 1992) are shown in Fig. 8. We start our analysis with garnet  
414 RTF-2 that shows an asymmetric OH<sup>-</sup> mode with a maximum at about 3650 cm<sup>-1</sup>. It could  
415 potentially, based on the arguments made above, represent a hydrogarnet substitution. However,  
416 its wavenumber is greater than any OH<sup>-</sup> mode measured in any end-member silicate garnet.  
417 Therefore, at first glance, it could be concluded that it does not represent a hydrogarnet  
418 substitution. However, there is explanation for its high wavenumber and it follows from an  
419 analysis of X-O bond lengths in binary X<sub>3</sub>Al<sub>2</sub>Si<sub>3</sub>O<sub>12</sub> garnet solid solutions (Bosenick et al., 2000;  
420 Freeman et al., 2006; Geiger, 2008). We propose that this OH<sup>-</sup> mode at roughly 3650 cm<sup>-1</sup>  
421 represents a hydropyrope-like cluster in a solid-solution silicate garnet crystal. The OH<sup>-</sup> mode is

422 greater by about  $20 \text{ cm}^{-1}$  wavenumbers than that for the  $\text{OH}^-$  mode in end-member pyrope ( $3629$   
423  $\text{cm}^{-1}$ ), because the associated Mg-O bonds in the hydropyrope cluster will be slightly greater in  
424 length compared to those in end-member silicate pyrope (note also that the wavenumber  
425 difference between the  $\text{OH}^-$  mode for katoite and  $\text{OH}^-$ -poor grossular (locally hydrogrossular  
426 clusters) is about  $60 \text{ cm}^{-1}$ ). That is, the presence of significant amounts of Ca in the garnet solid  
427 solution act to expand the average unit-cell volume compared to that in end-member pyrope and  
428 the Mg-O bonds will be slightly lengthened accordingly. It follows, then, that the  $\text{OH}^-$  stretching  
429 mode in a local hydropyrope cluster in a solid-solution crystal will be stronger and, thus, will  
430 vibrate at a higher energy compared to that of a local hydropyrope in nearly end-member pyrope.

431 Most mantle pyrope-rich garnets, though, are marked by the most intense  $\text{OH}^-$  mode  
432 located at approximately  $3570 \text{ cm}^{-1}$  (middle-wavenumber type of Bell and Rossman or group II of  
433 Matsuyk et al. - Fig. 8 samples RTF-4 and LAC 40 - and also see spectra “a” and “p” in Fig. 2 of  
434 Bell and Rossman, 1992). We assign this mode to a hydrogrossular-like-cluster contained in a  
435 pyrope-rich solid-solution crystal. The Ca-O bonds in the hydrogrossular cluster will be slightly  
436 shorter compared to those clusters in nearly end-member grossular and, thus, stronger. Therefore,  
437 the  $\text{OH}^-$  bond will be weaker and its stretching energy will lie at lower wavenumbers compared to  
438  $\text{OH}^-$  in nearly end-member grossular (i.e.,  $3598 \text{ cm}^{-1}$ ). The mass effect seems to play a secondary  
439 role in affecting the energy of this  $\text{OH}^-$  mode in the pyrope-rich solid solutions. Bell and Rossman  
440 (1992 - p. 169) write “Preliminary indications are that the position of this band maximum shifts in  
441 a regular fashion to lower wavenumber as a function of decreasing  $\text{Mg}/(\text{Mg} + \text{Fe})$  ratio in  
442 megacrysts.” We interpret this as indicating that the local hydrogrossular-like-clusters are  
443 becoming statistically slightly more  $\text{Fe}^{2+}$  rich (Fig. 6b). Finally, it is important to note that this  
444 band at  $3570 \text{ cm}^{-1}$  is often the most intense  $\text{OH}^-$  mode observed in the spectra of mantle pyropes  
445 (Bell and Rossman, 1998). We think this is reflecting the fact that a hydrogrossular cluster is  
446 energetically more favorable than say a hydropyrope cluster in a solid-solution garnet for the  
447 crystal-chemical reasons discussed above.

448 To end the analysis, we address the third major  $\text{OH}^-$  mode type that can be observed in mantle

449 pyropes. It is located at roughly  $3512\text{ cm}^{-1}$  (Bell and Rossman, 1992) or between  $3515\text{-}3527\text{ cm}^{-1}$   
450 (Matsuyk et al., 1998). The latter workers argue that this mode is associated with relatively  $\text{TiO}_2$ -  
451 rich garnets (about  $> 0.4\text{ wt. \%}$ ). This proposal is consistent with the IR spectra of synthetic Ti-  
452 bearing pyropes that have multi-OH-band spectra that show a low-energy mode at  $3526\text{ cm}^{-1}$  (Fig.  
453 8 –Geiger et al., 2000). It is also notable that these synthetic Ti-bearing pyropes show a broad OH  
454 mode at about  $3630\text{ cm}^{-1}$  at RT (Fig. 8), which splits into two narrow bands at 78 K (Geiger et al.,  
455 2000).

456

### 457 **Other Non-Hydrogarnet OH<sup>-</sup> Substitutional Mechanisms in End-Member Garnet**

458 The results and analysis given above are a strong argument that the hydrogarnet substitution can  
459 occur in several end-member or nearly end-member silicate garnets and that it is characterized by  
460 a single, broad OH<sup>-</sup> mode at RT. However, some nearly end-member natural garnets can also show  
461 more complex multi-OH<sup>-</sup>-band spectra, where the bands are relatively narrow and have energies  
462 unlike those garnets containing a hydrogarnet component (almandine - this work; pyrope - this  
463 work and Rossman et al., 1989; grossular - Rossman and Aines, 1991; spessartine - Aines and  
464 Rossman, 1984). The immediate conclusion is that there must be other structural or defect  
465 mechanisms for incorporating OH<sup>-</sup> in garnet. Figure 9 shows the IR spectrum of a nearly end-  
466 member pyrope (i.e., Masueria 2b - Table 1), a synthetic pyrope grown from a gel-starting  
467 material (Geiger et al., 1991), and a natural nearly end-member spessartine (Rutherford Mine,  
468 Amelia Courthouse, Amelia Co., VA). All three garnets show similar IR patterns with the same  
469 number of five OH<sup>-</sup> bands and having a similar wavenumber distribution (The OH<sup>-</sup> modes in  
470 spessartine lie at lower energies because, again,  $\text{Mn}^{2+}$  is heavier than  $\text{Mg}^{2+}$ ). The only difference is  
471 in the relative intensities among some of the bands. These three garnets apparently have OH<sup>-</sup>  
472 located at common structural sites and they are different than that of the “standard” hydrogarnet  
473 substitution. The narrow half widths of the OH<sup>-</sup> bands further characterize the spectra of these  
474 garnets and it can be argued that the vibrational freedom of the OH groups is more restricted  
475 compared to that for OH<sup>-</sup> groups in the hydrogarnet substitution.

476

477

## IMPLICATIONS

478 This work outlines how the hydrogarnet substitution can be identified in the IR spectra of nominally  
479 anhydrous end-member as well as some intermediate composition garnets. Low-temperature  
480 vibrational spectroscopic measurements are important in this determination. Spectra recorded at  
481 low-temperature are also necessary to fully understand the vibrational behavior (energetic and  
482 bonding) of H<sub>2</sub>O molecules occurring in various microporous silicates (e.g., Kolesov and Geiger,  
483 2002; 2005). It appears to be a common phenomenon that the large amplitudes of vibration  
484 associated with the light H atom in many OH<sup>-</sup> groups and H<sub>2</sub>O molecules in ionic crystals at RT  
485 causes a broadening of their respective vibrational modes. At low temperatures the vibrations are  
486 damped and these modes narrow and often split revealing more spectral and, thus, structural  
487 information.

488 A long and continuing goal in the investigation of H<sub>2</sub>O at low concentrations in nominally  
489 anhydrous silicates, and here garnet, is to assign different vibrational OH<sup>-</sup> stretching modes to  
490 various substitutional mechanisms and structural sites. The spectroscopic and crystal-chemical  
491 analysis undertaken in this work is a step in this direction. The results show that for silicates with  
492 relatively complex structures more effort must be made to understand local crystal-chemical  
493 properties and atomic configurations in the immediate vicinity of any OH<sup>-</sup> groups. This is necessary  
494 to interpret both the possible number of OH<sup>-</sup> modes as well as their energies. It follows, conversely,  
495 that it may be possible in some cases to use OH<sup>-</sup> stretching modes in nominally anhydrous minerals  
496 as a probe to investigate the nature of short-range-atomic order in intermediate solid-solution  
497 compositions (cf., to the case of OH-bearing minerals - Hawthorne and Della Ventura, 2007).

498 The role of atoms occurring in minor concentrations in garnet, especially those that lead to  
499 deviations in the nonstoichiometry of the formula unit from 3:2:3:12 (e.g., Na, B, Li, Zr, P, F), as  
500 well as possible point defects, and their possible effect on OH incorporation, needs further study.  
501 Work on compositionally simpler, well-characterized synthetic crystals will be essential in this

502 regard. Also important to consider is the role of trivalent cation substitutions at the tetrahedral site,  
503 where  $H^+$  may act as the charge-compensation ion associated with a single  $OH^-$  group.

504 Finally, the results and proposals, herein, could be of significance in terms of efforts to  
505 quantify the small concentrations of  $OH^-$  in garnet solid solutions. It can be expected that molar  
506 absorption coefficients for  $OH^-$  could be a function of the local structural type of  $OH^-$ . Existing  
507 calibrations with a single absorption coefficient, based on several  $OH^-$  modes deriving from  
508 different  $OH^-$  sites or groups (e.g., hydropyrope, hydrogrossular, hydrospessartine), may not be  
509 quantitative. It could be expected that each  $OH^-$  substitution mechanism (i.e., with different dipole  
510 interactions) will have its own characteristic molar absorption coefficient. The appears to be the  
511 case with olivine (Kovács et al., 2010). Concentrating calibration work just on the mode (or modes)  
512 related to a hydrogarnet substitution (or different local hydrogarnet substitutions in solid-solution  
513 crystals), as outlined herein, could permit a better understanding of  $OH^-$  concentration as a function  
514 of *P-T-X* crystallization conditions. Of course, any analytical method giving bulk  $OH^-$  contents  
515 could be difficult to interpret.

516

517

## ACKNOWLEDGMENTS

518 C. Chopin (Paris), C. Ferraris (Paris), J. Filip (Olomouc, Czech Republic) and A.B. Woodland  
519 (Frankfurt) generously donated crystals for study. This research was supported by two grants to  
520 C.A.G. from the Austrian Science Fund (FWF: P 25597-N20 and P30977-NBL) with a  
521 contribution from NSF grant EAR-1322082 to G.R.R. H. Skogby, an anonymous reviewer and the  
522 associate editor I. Kovács made constructive comments that improved the manuscript.

523

524

525

## REFERENCES

- 526 Adamo, I., Bocchio, R., Diella, V., Pavese, A., Vignola, P., Prosperi, L., and Palamza, V. (2009)  
527 Dematoid from Val Malenco, Italy: Review and update. *Gems and Gemology*, 45, 280-  
528 287.
- 529 Adamo, I., Gatta, G.D., Rotiroti, N., Diella, V., and Pavese, A. (2011) Green andradite stones:  
530 gemmological and mineralogical characterisation. *European Journal of Mineralogy*, 23, 91-  
531 100.
- 532 Aparicio, C., Filip, J., Skogby, H., Marusak, Z., Mashlan, M., and Zboril, R. (2012) Thermal  
533 behavior of almandine at temperatures of 1,200°C in hydrogen. *Physics and Chemistry of*  
534 *Minerals*, 39, 311-318.
- 535 Aines, R.D. and Rossman, G.R. (1984) The hydrous component in garnets: pyralspites. *American*  
536 *Mineralogist*, 69, 1116-1126.
- 537 Armbruster, T. and Lager, G.A. (1989) Oxygen disorder and the hydrogen position in garnet-  
538 hydrogarnet solid solution. *European Journal of Mineralogy*, 1, 363-369.
- 539 Armbruster, T. and Geiger, C.A. (1993) Andradite crystal chemistry, dynamic X-site disorder  
540 and strain in silicate garnets. *European Journal of Mineralogy*, 5, 59-71.
- 541 Armbruster, T., Geiger, C.A., and Lager, G.A. (1992) Single crystal X-ray refinement  
542 of almandine-pyrope garnets at 298 and 100 K. *American Mineralogist*, 77, 512-523.
- 543 Amthauer, G. and Rossman, G.R. (1998) The hydrous component in andradite garnet.  
544 *American Mineralogist*, 83, 835-840.
- 545 Bell, D.R. and Rossman, G.R. (1992) Water in Earth's mantle: the role of nominally  
546 anhydrous minerals. *Science*, 255, 1391-1397.
- 547 Bell, D.R. and Rossman, G.R. (1992) The distribution of hydroxyl in garnets from the  
548 subcontinental mantle of southern Africa. *Contributions to Mineralogy and Petrology*, 111,  
549 161-178.
- 550 Bosenick, A., Dove, M.T., and Geiger, C.A. (2000) Simulation studies of pyrope-grossular  
551 solid solutions. *Physics and Chemistry of Minerals*, 27, 398-418.

- 552 Cho., H. and Rossman, G.R. (1993) Single-crystal NMR studies of low-concentration hydrous  
553 species in minerals: Grossular garnet. *American Mineralogist*, 78, 1149-1164.
- 554 Chopin, C. (1984) Coesite and pure pyrope in high-grade blueschists of the Western Alps: a first  
555 record and some consequences. *Contributions to Mineralogy and Petrology*, 86, 107-118
- 556 Cohen-Addad, C., Ducros, P., and Bertaut, E.F. (1967) Étude de la substitution du  
557 groupement  $\text{SiO}_4$  par  $(\text{OH})_4$  dans les composés  $\text{Al}_2\text{Ca}_3(\text{OH})_{12}$  et  
558  $\text{Al}_2\text{Ca}_3(\text{SiO}_4)_{2.16}(\text{OH})_{3.36}$  de type grenat. *Acta Crystallographica*, 23, 220-230.
- 559 Flint, E.P., McMurdie, H.F., and Wells, L.S. (1941) Hydrothermal and X-ray studies of the  
560 garnet-hydrogarnet series and the relationship of the series to hydration products of  
561 portland cement. *Journal of Research of the National Bureau of Standards*, 27, 171-  
562 180.
- 563 Foreman, D.W. Jr. (1968) Neutron and X-ray diffraction study of  $\text{Ca}_3\text{Al}_2(\text{O}_4\text{D}_4)_3$ , a garnetoid.  
564 *The Journal of Chemical Physics*, 48, 3037-3041.
- 565 Freeman, C.L., Allan, N.L., and van Westrenen, W. (2006) Local cation environments in the  
566 pyrope-grossular  $\text{Mg}_3\text{Al}_2\text{Si}_3\text{O}_{12}$ - $\text{Ca}_3\text{Al}_2\text{Si}_3\text{O}_{12}$  garnet solid solution. *Physical Review*, 74,  
567 134203-1-134203-9.
- 568 Geiger, C.A. (2008) Silicate garnet: A micro to macroscopic (re)view. *American*  
569 *Mineralogist*, 93, 360-372.
- 570 Geiger, C.A. and Armbruster, T. (1997)  $\text{Mn}_3\text{Al}_2\text{Si}_3\text{O}_{12}$  spessartine and  $\text{Ca}_3\text{Al}_2\text{Si}_3\text{O}_{12}$  grossular  
571 garnet: dynamical structural and thermodynamic properties. *American Mineralogist*,  
572 82, 740-747.
- 573 Geiger, C.A. and Rossman, G.R. (1994) Crystal field stabilization energies of almandine-pyrope  
574 and almandine-spessartine garnets determined by FTIR near infrared measurements. *Physics*  
575 *and Chemistry of Minerals*. 21, 516-525.
- 576 Geiger, C.A., Langer, K., Bell, D.R., Rossman, G.R., and Winkler, B. (1991) The hydroxide  
577 component in synthetic pyrope. *American Mineralogist*, 76, 49-59.

- 578 Geiger, C.A., Stahl, A., and Rossman, G.R. (2000) Single-crystal IR- and UV/ VIS-  
579 spectroscopic measurements on transition-metal-bearing pyrope: The incorporation of  
580 hydroxide in garnet. *European Journal of Mineralogy*, 12, 259-271.
- 581 Geiger, C.A., Dachs, E., Vielreicher, N. and Rossman, G.R. (in press) Heat capacity behavior of  
582 andradite: A multi-sample and -methodological investigation. *European Journal of*  
583 *Mineralogy*.
- 584 Hawthorne, F.C. and Della Ventura, G. (2007) Short-range order in amphiboles. In F.C.  
585 Hawthorne, R. Oberti, G. Della Ventura, and A. Mottana, Eds., *Amphiboles: Crystal*  
586 *Chemistry, Occurrence, and Health Issues*, 67, p. 173-222. *Reviews in Mineralogy and*  
587 *Geochemistry*, Mineralogical Society of America, Chantilly, Virginia.
- 588 Hösch, A. and Langer, K. (1996) Single crystal MFTIR-spectra at various temperatures of  
589 synthetic end member garnets in the OH-valence vibrational region. *Physics and*  
590 *Chemistry of Minerals*, 23, 305-306.
- 591 Keppler, H., and Smyth, J.R. (2006) Water in nominally anhydrous minerals. (eds) *Reviews*  
592 *in Mineralogy and Geochemistry* 62, Mineralogical Society of America, 169-191.
- 593 Kolesov, B.A. and Geiger, C.A. (2002) Raman spectroscopic study of H<sub>2</sub>O in bikitaite: “One-  
594 dimensional” ice. *American Mineralogist*. 87, 1426-1431.
- 595 Kolesov, B.A. and Geiger, C.A. (2005) The vibrational spectrum of synthetic hydrogrossular  
596 (Katoite) Ca<sub>3</sub>Al<sub>2</sub>(O<sub>4</sub>H<sub>4</sub>)<sub>3</sub>: A low temperature IR and Raman spectroscopic study.  
597 *American Mineralogist*. 90, 1335-1341.
- 598 Kovács, I., O'Neill H. St. C., Hermann J., Hauri, E. (2010): Site-specific infrared O-H  
599 absorption coefficients for water substitution into olivine. *American Mineralogist*, 95,  
600 292-299.
- 601 Lager, G.A., Armbruster, T., and Faber, G. (1987) Neutron and X-ray diffraction study of  
602 hydrogarnet Ca<sub>3</sub>Al<sub>2</sub>(O<sub>4</sub>H<sub>4</sub>)<sub>3</sub>. *American Mineralogist*, 72, 756-765.

- 603 Lager, G.A., Downs, R.T., Origlieri, M., and Garoutte, R. (2002) High-pressure single-crystal  
604 X-ray study of katoite hydrogarnet: Evidence for a phase transition from  $Ia3d \rightarrow I43d$   
605 symmetry at 5 GPa. *American Mineralogist*, 87, 642-647.
- 606 Libowitzky, E. (1999) Correlation of O-H stretching frequencies and O-H...O hydrogen bond  
607 lengths in minerals. *Monatshefte für Chemie*, 130, 1047-1059.
- 608 Lutz, H.D. (1988) Bonding and structure of water molecules in solid hydrates. Correlation of  
609 spectroscopic and structural data. *Structure and Bonding*, 69, p. 97-125. Springer-Verlag,  
610 New York.
- 611 Mookerjee, M. and Karato, S. (2010) Solubility of water in pyrope-rich garnet at high pressures  
612 and temperature: *Geophysical Research Letters*, 37, L03310, 1-5.
- 613 Matsyuk, S.S., Langer, K., and Hösch, A. (1998) Hydroxyl defects in garnets from mantle  
614 xenoliths in kimberlites of the Siberian platform. *Contributions to Mineralogy and*  
615 *Petrology*, 132, 163-179.
- 616 Nakamoto, K., Margoshes, M., and Rundle, R.E. (1955) Stretching frequencies as a function of  
617 distances in hydrogen bonds. *Journal of American Chemical Society*, 77, 6480-6486.
- 618 Palke, A.C., Stebbins, J.F., Geiger, C.A., and Tippelt, G. (2015) Cation order-disorder in Fe-  
619 bearing pyrope and grossular garnets: An  $^{27}\text{Al}$  and  $^{29}\text{Si}$  MAS NMR and  $^{57}\text{Fe}$  Mössbauer  
620 spectroscopy study. *American Mineralogist*, 100, 536-547.
- 621 Pigott, J.S., Wright, K., Gale, J.D., and Panero, W.R. (2015) Calculation of the energetics of  
622 water incorporation in majorite garnet. *American Mineralogist*, 100, 1065-1075.
- 623 Rossman, G.R. and Aines, R.D. (1991) The hydrous components in garnets: Grossular-  
624 hydrogrossular. *American Mineralogist*, 76, 1153-1164.
- 625 Rossman, G.R., Beran, A., and Langer, K. (1989) The hydrous component of pyrope from the  
626 Dora Maira Massif, Western Alps. *European Journal of Mineralogy*, 1, 151-154.
- 627 Simon, G. and Chopin, C. (2001) Enstatite-sapphirine crack-related assemblages in ultrahigh-  
628 pressure pyrope megablasts, Dora Maira Massif, western Alps. *Contributions to Mineralogy*  
629 *and Petrology*, 140, 422-440.

- 630 Soucek, J. (1978) Metamorphic zones of the Vrbno and Rejviz Series, the Hruby Jesenik  
631 Mountains, Czechoslovakia. *Tschermaks Mineralogische und Petrographische Mitteilungen*,  
632 25, 195-217.
- 633 Thomas, S-M., Wilson, K., Koch-Müller, M., Hauri, E.H., McCammon, C., Jacobsen, S.D.,  
634 Lazarz, J., Rhede, D., Ren, M., Blair, N., and Lenz, S. (2015) Quantification of water in  
635 majoritic garnet. *American Mineralogist*, 100, 1084-1092.
- 636 Withers, A.C., Wood, B.J., and Carroll, M.R. (1998) The OH content of pyrope at high pressure.  
637 *Chemical Geology*, 147, 161-171.
- 638 Woodland, A.B., Droop, G., and O'Neill, H.St.C. (1995) Almandine-rich garnet from  
639 Collobrières, southern France, and its petrological significance. *European Journal of*  
640 *Mineralogy*, 7, 187-194.
- 641
- 642
- 643

644 Table 1. Description of natural and synthetic garnet samples measured in this study.

Sample Label	Locality (Source)/ Synthesis Conditions/ Composition	Sample Description & Composition	Mole % ( $\pm 1-2$ ) End Member
Pyrope MAS-2a	Masueria, Italy (Ch. Chopin; Simon & Chopin, 2001; Geiger & Rossman, 1994)	Pinkish to light red transparent single crystal containing various inclusions.	Py(76)
Pyrope MAS-2b	Masueria, Italy (Ch. Chopin; Simon & Chopin, 2001, Geiger & Rossman, 1994)	Very light pinkish transparent single crystal.	Py(99)
Pyrope SB	San Bernardo, Italy (Ch. Chopin; Simon & Chopin, 2001; Geiger & Rossman, 1994)	Light pinkish transparent single crystal.	Py(82)
Pyrope Ch-2	“Dora Maira”, Italy (Ch. Chopin, exact locality unknown; Geiger & Rossman, 1994)	Colorless transparent single crystal.	Py(98)
Andradite #27	$T = 1200\text{ }^{\circ}\text{C}$ & $P = 20\text{ kbar}$ , w/ $\text{PtO}_2$ (Armbruster & Geiger, 1993; Geiger et al., submitted)	Loose synthetic polycrystalline product ( $\text{An}_{100}$ ) with some individual crystals up to roughly $300\text{ }\mu\text{m}$ in size. Yellow greenish to golden in color. Isotropic.	An(100)

Andradite GRR-134	Val Malenco, Italy (Amthauer & Rossman, 1998)	Light green transparent single crystal. Anisotropic.	An(99)
Almandine A-5	Collobrières, France (C. Ferraris, Paris, Muséum national d'histoire naturelle, Geiger & Rossman, 1994)	Single crystals mm size. Compositionally homogeneous and unzoned. Inclusions.	Al(94)
Almandine FR-3	Collobrières, France (Woodland et al., 1995)	Crystals up to cm size. Metamorphosed ironstone. Compositionally homogeneous and unzoned. Numerous cracks and some inclusions.	Al(93)
Almandine JF-1	Zlaty Chlum near Jeseník, Czech Republic (Aparicio et al., 2012)	Metasedimentary rocks.	Al(95)

645  
646  
647  
648

## Figures

649

650

651 Figure 1. IR single-crystal spectra of natural end-member andradite from Val Malenco, Italy,  
652 (Table 1) at 296 K, 198 K, 123 K, 89 K and 80 K (from bottom to top). The broad asymmetric OH  
653 band at room temperature has a peak maximum at  $3563\text{ cm}^{-1}$  and two major peaks at  $3575\text{ cm}^{-1}$   
654 and  $3557\text{ cm}^{-1}$  at 80 K. The RT spectrum of synthetic andradite #27 (black) is shown at the bottom  
655 (Geiger et al., in press) also with a single band at  $3563\text{ cm}^{-1}$  at RT.

656

657 Figure 2. IR single-crystal spectra of various composition pyrope-rich crystals from Dora Maira,  
658 Italy (Table 1). They are shown with increasing almandine and slight grossular contents (decreasing  
659 pyrope component) from bottom to top. For the most “water-rich” crystal (Masueria 2b) the five  
660 main OH band energies are at  $3660$ ,  $3651$ ,  $3641$ ,  $3618$  (weak) and  $3602\text{ cm}^{-1}$  and a weak shoulder  
661 on the high-energy wing of the band at  $3660\text{ cm}^{-1}$ . The OH modes broaden with decreasing pyrope  
662 content in more intermediate compositions due to variations in local atomic configurations (see  
663 text).

664

665 Figure 3. IR single-crystal spectra of the three almandine-rich crystals (Table 1). The sample FR-3  
666 is 0.30 mm, sample A-5 0.22 mm, and sample JF-1 0.36 mm thick. The sloping background is due  
667 to the low-energy flank of an intense electronic transition related to  $\text{Fe}^{2+}$  that is centered at about  
668  $4400\text{ cm}^{-1}$  (Geiger and Rossman, 1994). The OH band energies are given in the text.

669

670 Figure 4. Comparison of IR spectra of end-member synthetic pyrope (sample P-13, 0.273 mm  
671 thick, from Geiger et al., 1991), almandine (A-2,  $\sim 0.90$  mm thick, in Geiger et al., in press) and  
672 natural andradite (GRR-134, 1.185 mm thick, this work) at room temperature and  $\sim 80\text{ K}$  (liquid  
673  $\text{N}_2$ ). For synthetic pyrope the OH band at  $3629\text{ cm}^{-1}$  at RT splits into two narrow OH bands at  
674  $3638$  and  $3614\text{ cm}^{-1}$ . For synthetic almandine the most intense broad OH band at  $3613\text{ cm}^{-1}$  at RT

675 splits into three narrow OH bands at 3663 (weakest), 3617 (intense) and 3590 (weak)  $\text{cm}^{-1}$  at about  
676 80 K with the latter two assumed to represent the hydrogarnet substitution.

677

678 Figure 5. Local atomic environment around a single OH dipole in the case of katoite (no Si  
679 cation). The oxygen anion (red) in the garnet structure is bonded to one Y(Al) cation (blue), two  
680 X(Ca) cations (yellow - in hydrogrossular with bond lengths of  $\text{Ca1-O(1)} = 2.462(3) \text{ \AA}$  and  $\text{Ca(2)-}$   
681  $\text{O(4)} = 2.520(3) \text{ \AA}$  (Lager et al., 2002) and a H atom (pink).

682

683 Figure 6. a.) Hypothetical tetrahedral-dodecahedral “chain” that could be found in a Mg-Fe-Ca  
684 intermediate composition garnet. Both  $\text{O}_4\text{H}_4$  (H atoms are the pinkish-colored spheres) and  $\text{SiO}_4$   
685 (red) “tetrahedra” are shown. For example, in the case of a pyrope-rich solid-solution crystal, the  
686 yellow spheres would represent Mg, brown  $\text{Fe}^{2+}$  and green Ca. b.) One hypothetical local divalent  
687 X-cation environment around an  $\text{O}_4\text{H}_4$  group in garnet. The oxygen anions from each of the four  
688  $\text{OH}^-$  dipoles form the central tetrahedron and they can be bonded locally to different combinations  
689 of X-cations. This can lead to  $\text{OH}^-$  mode broadening in solid-solution crystals (see text).

690

691 Figure 7. IR spectra of  $\text{Mg}_3\text{Al}_2\text{Si}_3\text{O}_{12}$  (P-13 - Geiger et al., 1991) synthesized at  $P(\text{H}_2\text{O}) = 2.3 \text{ Ga}$   
692 and  $T = 1100 \text{ }^\circ\text{C}$  and garnet of composition  $(\text{Mg}_{2.50}\text{Fe}^{2+}_{0.59})(\text{Si}_{0.06}\text{Al}_{1.76}\text{Cr}_{0.08}\text{Fe}^{3+}_{0.02})\text{Si}_3\text{O}_{12}$   
693 (spectrum MA384 digitized from Thomas et al., 2015, with absorbance divided by 30) synthesized  
694 at  $P(\text{H}_2\text{O}) = 18 \text{ GPa}$  and  $T = 1800 \text{ }^\circ\text{C}$  (with  $0.5 \text{ }\mu\text{L H}_2\text{O}$  added). The  $\text{OH}^-$  band defines a local  
695 hydropyrope cluster in both crystals.

696

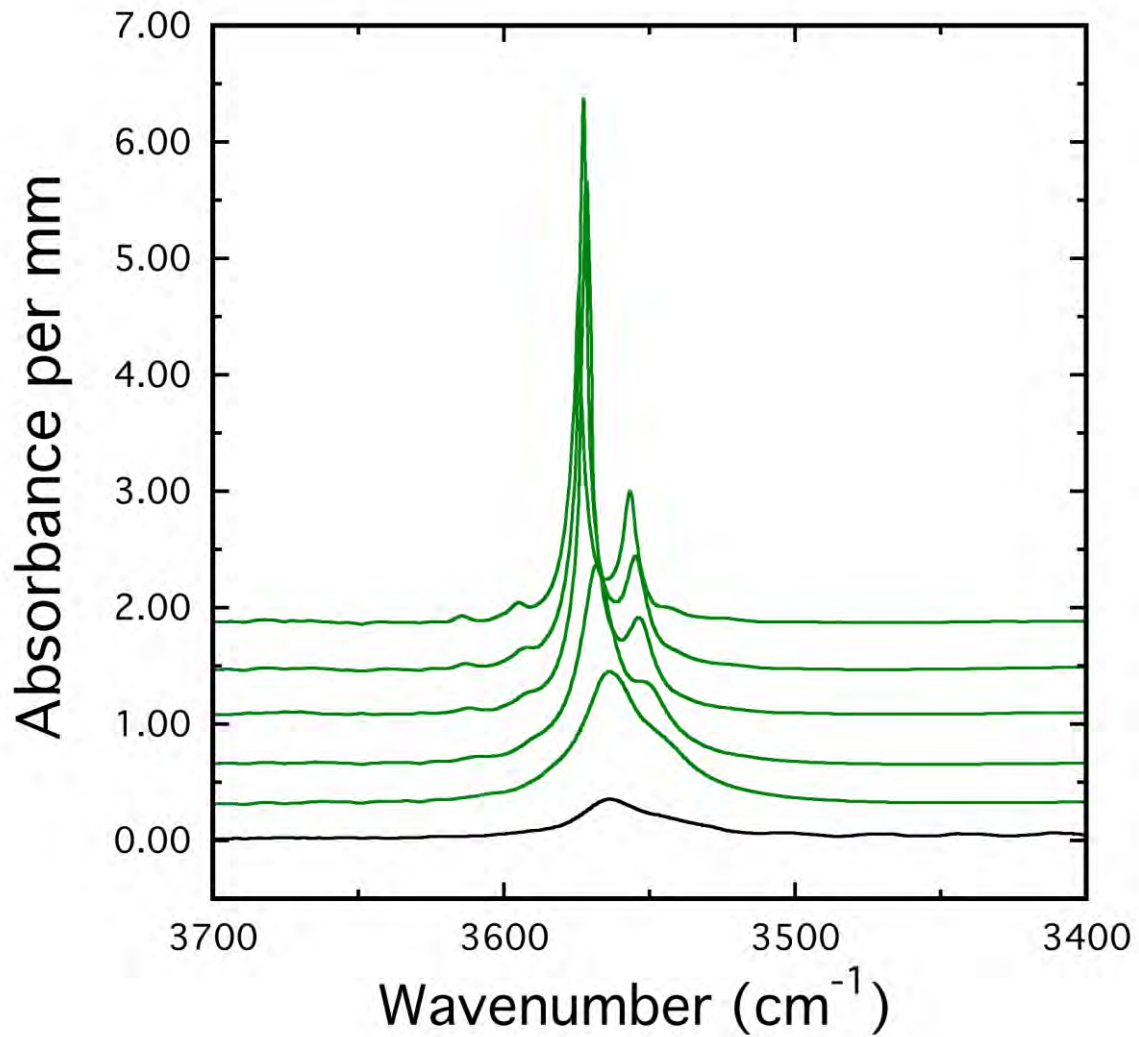
697 Figure 8. Comparison of IR spectra of two synthetic and three natural pyropes. The synthetic Ti-  
698 bearing pyrope is from Geiger et al. (2000) and end-member pyrope from Geiger et al. (1991). The  
699 IR spectra for the three natural pyropes are from Bell and Rossman (1992, note that the IR spectra  
700 for RTF-2 and RTF-4 are interchanged in their work). The garnets show their three different

701 wavenumber types “high, middle and low” or the I, II and III groups of Matsuyk et al. (1998). The  
702 three types or groups are marked by red, blue and green arrows, respectively. The red arrow marks  
703 a possible local hydropyrope cluster in the garnet (about  $3630\text{ cm}^{-1}$  in the synthetics and  $3650\text{ cm}^{-1}$   
704 in the natural solid solution RTF-2). The blue arrow marks a possible hydrogrossular-like cluster  
705 in RTF-4 and LAC-40 (at about  $3570\text{ cm}^{-1}$ ). The green arrow marks an OH mode possibly related  
706 to the presence of Ti in garnet. See text for further discussion.

707  
708 Figure 9. IR spectra of natural end-member spessartine (GRR-43 - 0.271 mm), natural end-  
709 member pyrope (Masueria 2b - 2.308 mm) and pyrope synthesized from a gel (Py-27 in Geiger et  
710 al., 1991, normalized to 5.0 mm). The latter has bands at 3663, 3651, 3641, and 3618 and a low  
711 energy shoulder at  $3604\text{ cm}^{-1}$  and also a weak shoulder on the high energy wing of the band at  
712  $3663\text{ cm}^{-1}$ .

713

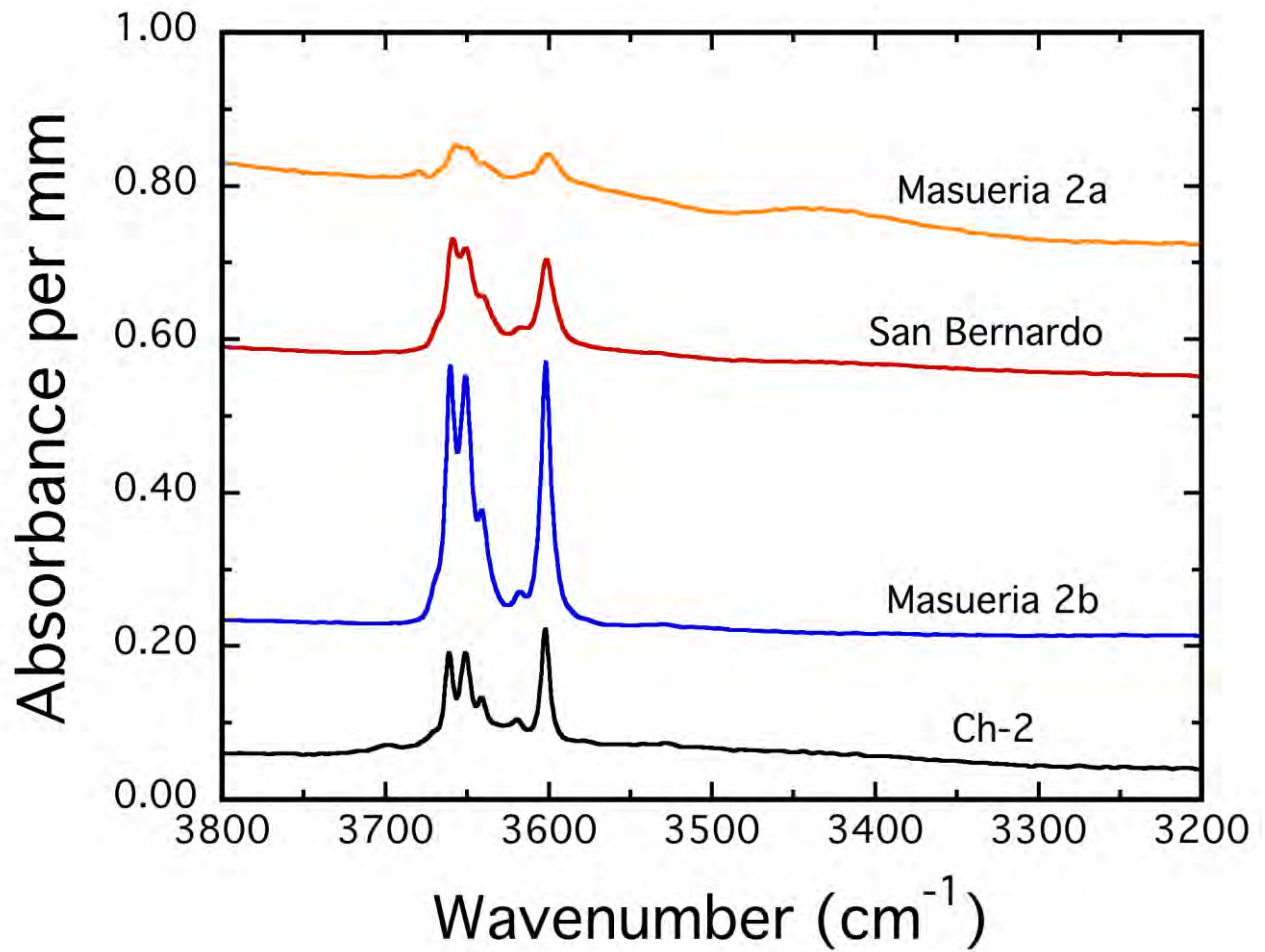
714  
715  
716  
717  
718  
719  
720



721  
722  
723  
724  
725  
726  
727  
728  
729  
730  
731  
732  
733  
734  
735  
736

Fig. 1

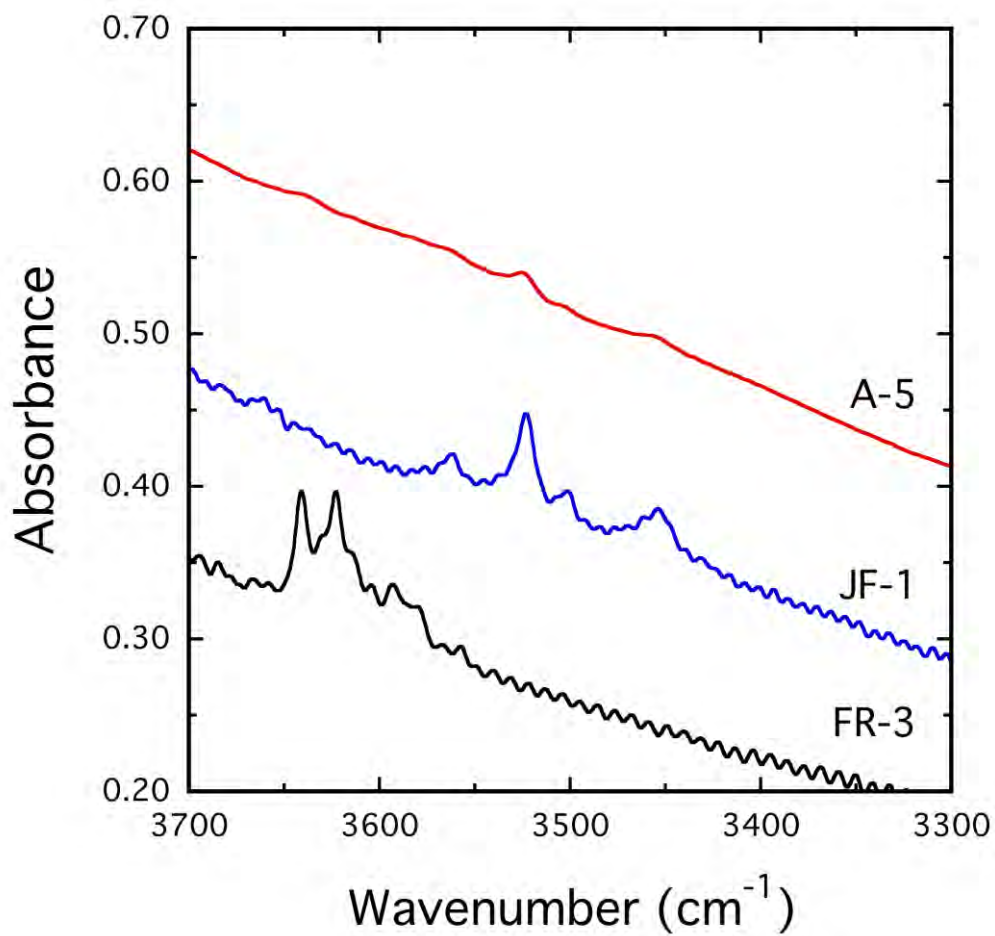
737  
738  
739  
740



741  
742  
743  
744  
745  
746  
747  
748  
749  
750  
751  
752  
753  
754

Fig. 2

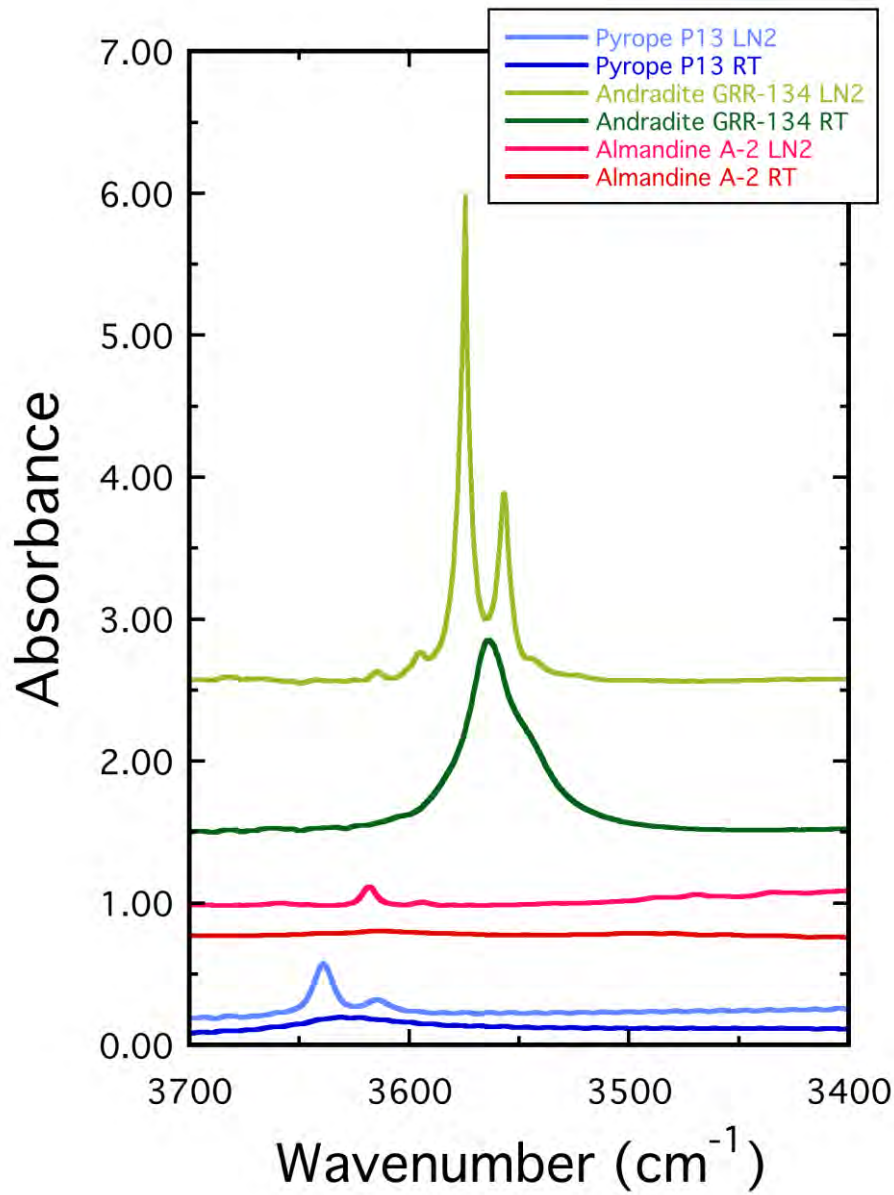
755  
756  
757  
758



759  
760  
761  
762  
763  
764  
765  
766  
767  
768  
769  
770  
771  
772

Fig. 3

773  
774  
775

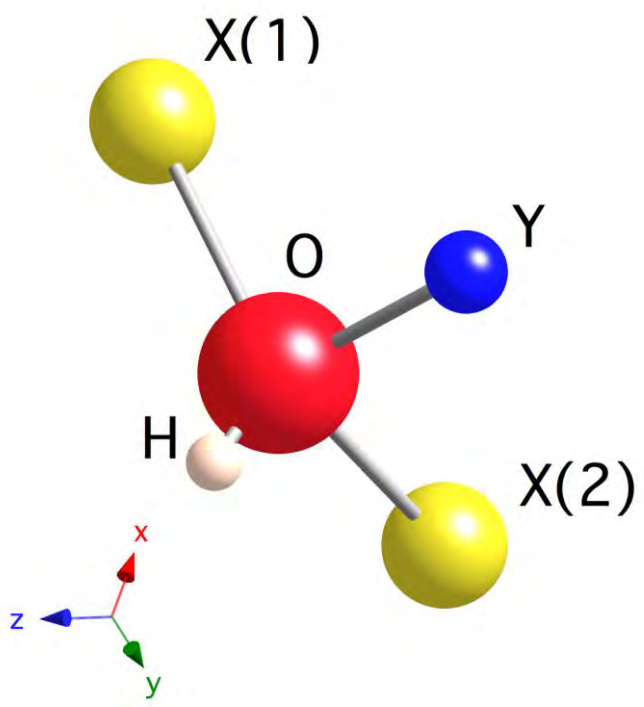


776  
777  
778  
779  
780  
781  
782  
783  
784  
785

Fig. 4

786  
787  
788  
789

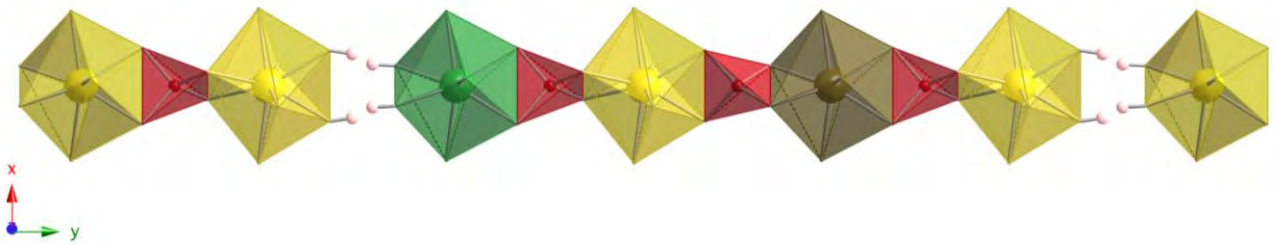
790



812  
813  
814  
815  
816  
817  
818  
819  
820  
821  
822  
823  
824  
825  
826  
827  
828  
829  
830  
831  
832  
833  
834  
835  
836

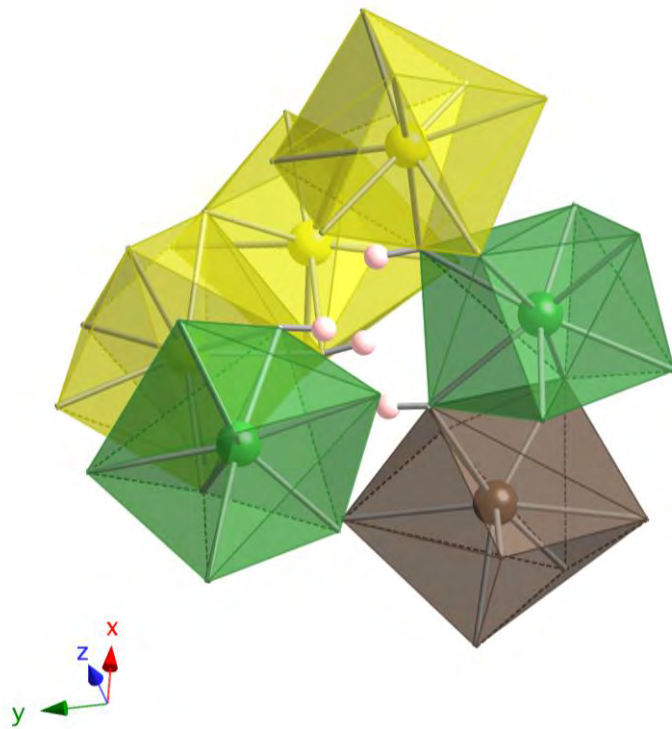
Fig. 5

837  
838  
839  
840  
841



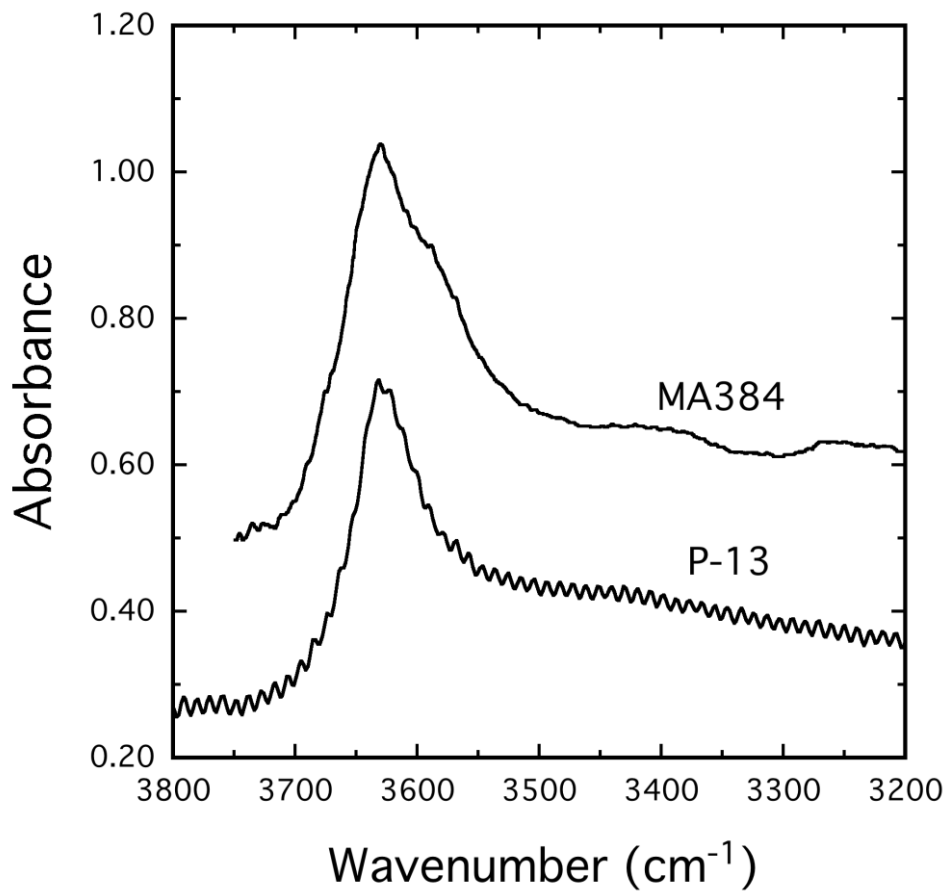
842  
843  
844  
845  
846  
847  
848 a.)

849  
850  
851  
852  
853



854  
855  
856  
857  
858 b.)  
859  
860 Fig. 6

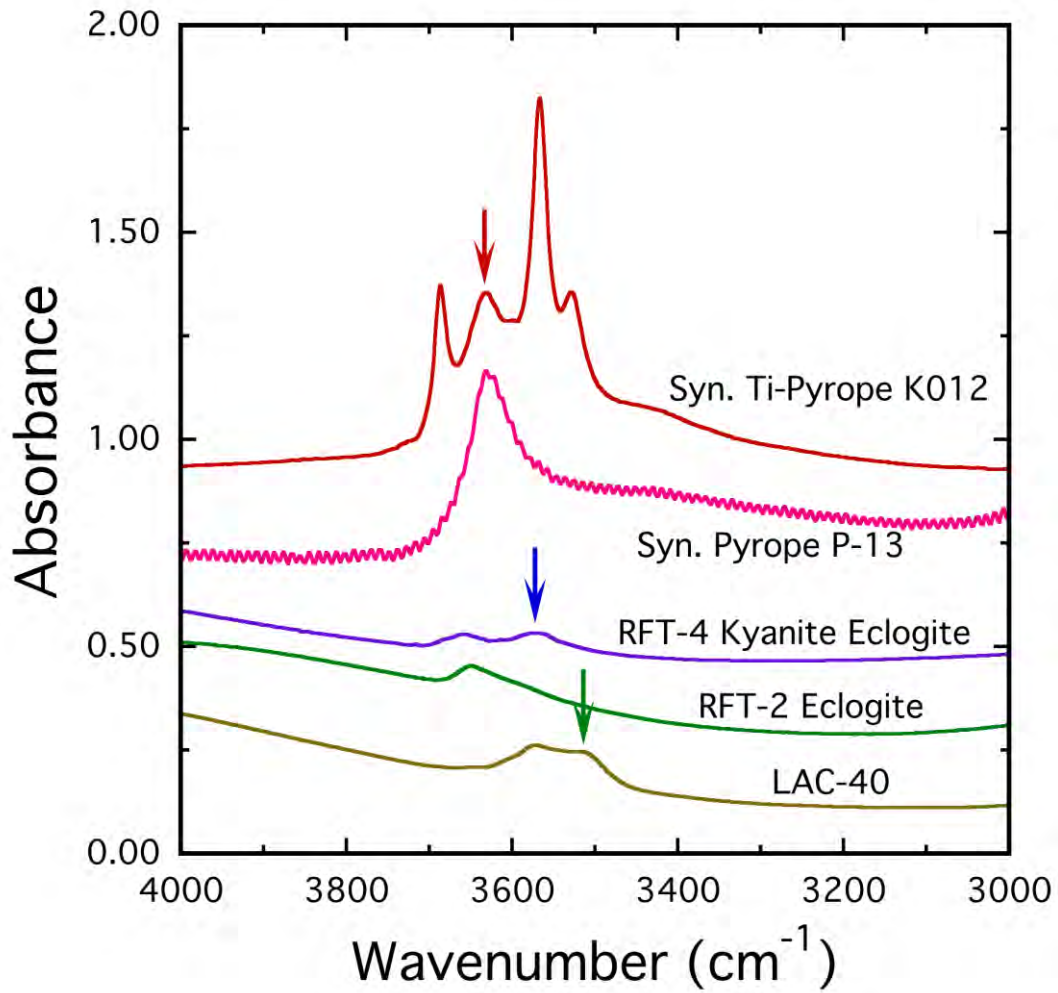
861  
862  
863  
864  
865  
866



867  
868  
869  
870  
871  
872  
873  
874  
875  
876  
877  
878  
879  
880  
881  
882  
883  
884  
885  
886  
887  
888

Fig. 7

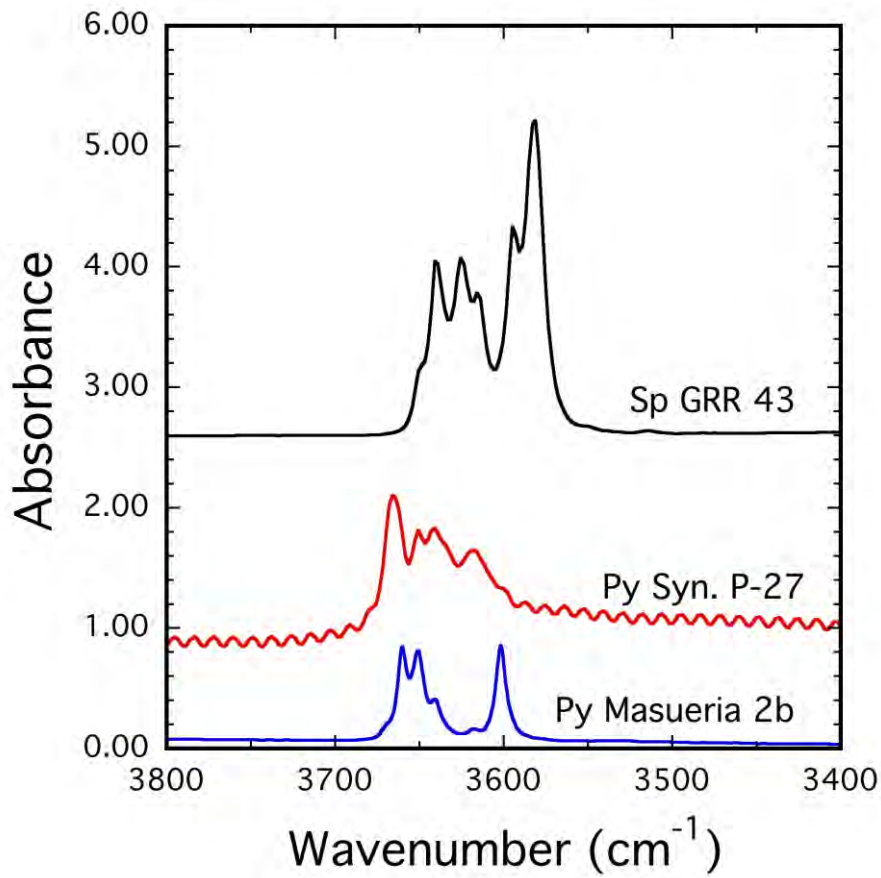
889  
890  
891  
892  
893  
894  
895



896  
897  
898  
899  
900  
901  
902  
903  
904  
905  
906  
907  
908  
909  
910  
911  
912  
913

Fig. 8

914  
915  
916  
917  
918



919  
920  
921  
922  
923  
924  
925  
926  
927  
928  
929  
930  
931  
932  
933  
934

Fig. 9